

# Reconstruction of sea surface temperatures from the oxygen isotope composition of fossil planktic foraminifera

Jan Bouwe van den Berg, Natalia Davydova, Barbera van de Fliert,  
Frank Peeters, Bob Planqué, Harmen van der Ploeg, Guido Terra.

**ABSTRACT.** Knowledge of the historic surface temperature of sea water is of importance for the calibration of climate models. The oxygen isotope composition of the shells of several species of planktic foraminifera can be used as a measure for this sea surface temperature. In this paper we investigate how mathematical models can contribute to the process of extracting information about the temperature at which the foraminifera lived from measurement of the oxygen isotope composition of their shells. A simple model is proposed which captures both the average and the variability of the temperature. Preliminary findings suggest that this model forms a solid basis for future research.

**KEYWORDS:** Historic sea surface temperature, foraminifera, oxygen isotope composition, mathematical models

## 1. Introduction

With the ongoing debate on global warming of the last decades, the need for a solid understanding of the variability of the world's climate is a hot issue. To assess such changes researchers often use climate models to predict the climate of the future. Predictions of future climate conditions are based upon knowledge of current and past conditions. The more detailed and accurate this knowledge, the better the prediction. One of the many components of climate models is the surface temperature of sea water. To be able to predict sea surface temperatures for the future, knowledge of sea surface temperatures of the past is thus essential. Here we propose to use the chemical composition of fossil shells of planktic foraminifera to reconstruct past sea surface temperatures and their variability. We investigate several mathematical models that can be used to perform this task.

In sections 1.1–1.5 we discuss various aspects of the background information on planktic foraminifera and their dependence on the sea surface temperature. In section 2 a basic model is presented and the

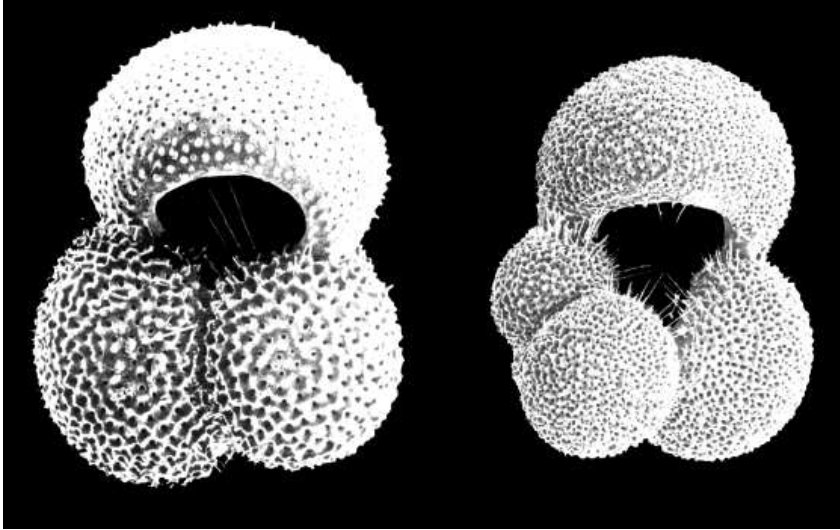


FIGURE 1. Scanning Electron Microscope image of the shells of two species of planktic foraminifera: *Globigerinoides ruber* (left) and *Globigerina bulloides*. The shells were collected in the surface waters of the Arabian Sea. The shells have a diameter of about  $300\ \mu\text{m}$ .

reconstruction via this model of the sea surface temperature from the experimental data is carried out in detail. A more sophisticated model describing the population dynamics in terms of a system of ordinary differential equations is discussed in section 3 and it is explained how this in principle can be used to analyse the experimental data. Finally, in section 4 we discuss our findings and give perspectives on possible further research.

**1.1. Planktic foraminifera.** Planktic foraminifera are small marine unicellular organisms with a shell made of calcite ( $\text{CaCO}_3$ ). As opposed to benthic foraminifera which live on the sea floor, planktic foraminifera float in the upper water column. The shells of planktic foraminifera are between  $50 - 500\ \mu\text{m}$  in diameter and function as their skeleton, see Figure 1. Depending on the taxonomic perspective (it is not always easy to decide whether differences are sufficient to justify a division into separate species), this group of marine microzooplankton comprises about 40 currently living species [2]. At the end of their life cycle of about four weeks the organisms reproduce, die, and subsequently sink to the sea floor. Consequently, the sediments found on the ocean floor contain a large number of fossil shells of different species.

These sediments serve as a geological archive that can be used to extract environmental information of the ancient upper water column such as, for example, the sea surface temperature. This is possible since the temperature of the ambient sea water is recorded in the oxygen isotopic composition of the shells during the life cycle of a foraminifer.

A number of methods have been developed to determine the ancient temperatures of the upper ocean. Such models do not use the chemical composition of the shells, but only make use of the relative abundance of different species. These methods assume that there is a relationship between fossil faunas found in the uppermost part of the ocean floor sediments and present-day physical conditions in the ocean (e.g. see [6] and references therein). On a wide range of observations multivariate statistical techniques are used to establish a relationship between the relative abundance of different species and the sea surface temperature. This statistical relationship is then used for older sediment layers to reconstruct climatic changes over time. They rely on empirical statistical correlation and do not include ecological information of the organisms considered. We try to improve on these investigations by developing a model that encompasses some basic ecology of the foraminifera and uses the oxygen composition of their shells to reconstruct sea surface temperatures.

**1.2. Oxygen isotope composition of  $\text{CaCO}_3$  and its relationship to temperature.** There are several naturally occurring isotopes of oxygen. The main stable isotope is  $^{16}\text{O}$ , which has a natural abundance of 99.76%; the next most abundant isotope is  $^{18}\text{O}$ . The oxygen isotope composition of a substance is given in conventional delta-notation as ‰ deviation from a given standard, the so-called PDB standard (that is the isotopic composition of  $\text{CO}_2$  gas produced with phosphoric acid from a Cretaceous belemnite (*Belemnitella americana*) of the Peedee Formation of South Carolina [14]):

$$\delta^{18}\text{O}_{\text{sample}} = \frac{(^{18}\text{O}/^{16}\text{O})_{\text{sample}} - (^{18}\text{O}/^{16}\text{O})_{\text{standard}}}{(^{18}\text{O}/^{16}\text{O})_{\text{standard}}} \cdot 1000 \text{ ‰}.$$

The isotopic composition of the calcite shells of foraminifera,  $\delta^{18}\text{O}_C$ , depends on the isotopic composition of the water in which they live,  $\delta^{18}\text{O}_W$ , the sea surface temperature  $T$ , and a so-called vital effect  $\delta^{18}\text{O}_{VE}$  (modified after [4]):

$$(68) \quad \delta^{18}\text{O}_C = 25.778 - 3.333 \cdot (43.704 + T)^{0.5} + \delta^{18}\text{O}_W + \delta^{18}\text{O}_{VE}.$$

The vital effect is a species-specific correction term. Although the mechanisms causing this offset is not well-understood, the vital effect is relatively well-known from field observations [10]. In this study we

assume that the vital effect for a given species is constant over the sea water temperature range, i.e.  $0 - -30^{\circ}\text{C}$ . The composition of the sea water varies on a much larger time scale than its temperature. Thus, if one performs experiments with currently living organisms, one takes the  $\delta^{18}\text{O}_W$  to be a known constant. The change in the oxygen isotopic ratio of the calcite shell is about a 0.2‰ decrease for each degree of temperature increase. This is sufficient for us to be able to estimate the temperature of the water in which the organisms lived. Thus, by measuring the oxygen isotope composition of a foraminifer shell  $\delta^{18}\text{O}_C$ , one can determine the temperature of the water in which the organism built its shell, given the oxygen isotope composition of the sea water  $\delta^{18}\text{O}_W$ .

In this study, we make use of the oxygen isotope composition of three species that live in the uppermost layers of the ocean: *Globigerina bulloides*, *Globigerinoides ruber* and *Neogloboquadrina dutertrei*. Based on field observations the vital effect of these species are:  $-0.41\text{‰}$  for *G. bulloides*,  $-0.45\text{‰}$  for *G. ruber* and  $-0.01\text{‰}$  for *N. dutertrei*. Although these species often occur simultaneously in tropical waters, their ecology differs considerably. For example, *G. bulloides* prefers relatively cool food-rich water, between  $3$  and  $19^{\circ}\text{C}$ , such as found at high latitudes (Arctic and Sub-arctic) and in (tropical) upwelling areas. The species *G. ruber*, however, favours relatively food-poor and warmer water between  $13$  and  $32^{\circ}\text{C}$ , while the temperature range of *N. dutertrei* is estimated to be between  $15$  and  $25^{\circ}\text{C}$ .

**1.3. Towards an Isotopic Transfer Function.** The main objective of this study is to reconstruct sea surface temperatures of the past using data on the oxygen isotope composition of different species of foraminifer shells. Equation (68) would be a good first candidate, but cannot be applied directly because no accurate information on the oxygen composition of the sea water from past times is available. This makes a direct inference of the temperature from the calcite composition of an individual shell theoretically impossible.

Naively, this problem seems to be overcome when we subtract two such equations by comparing the isotope composition of shells of two species: this would eliminate the  $\delta^{18}\text{O}_W$  from the equation. But, apart from the vital effect  $\delta^{18}\text{O}_{VE}$ , the relation (68) is the same for each species. Hence one does not expect this difference to contain any information. However, due to differences in the ecological preferences of the different species, the temperature recorded in their shells according to formula (68) is not the same for all species. Since the different species of planktic foraminifera do not prefer the same environmental conditions, the production patterns of different species will vary in the course of the

year. For example, it can be expected that “cold loving” species will produce their shells preferably during the cool period of the year, whereas the shell production of “warm loving” species will be biased towards the warm period of the year. Consequently, the isotopic composition of a given species reflects the temperature of the sea water during that part of the year for which environmental conditions were optimal.

A single sample from the cores represents about 100 years, whereas the life span of a foraminifer is a few weeks. For an isotopic analysis of a species about 20 shells are needed. This means that one only obtains (yearly) averaged values. For each species these averages will be biased towards that part of the year during which the environmental conditions were most favourable to them. In an open oceanic setting the  $\delta^{18}\text{O}_W$ -value is relatively constant on seasonal to decadal time scales. We therefore may assume that the different species have experienced the same  $\delta^{18}\text{O}_W$ . Hence by subtracting two such averages the  $\delta^{18}\text{O}_W$ -value drops out. This idea has first been proposed by [8, 9]. The differences between the isotopic composition of different species, corrected for their vital effect, must be explained by their difference in calcification temperature. This difference is determined by: 1) the ecology of the species under consideration and 2) the environmental conditions in the upper ocean throughout the year. The relation between the environmental conditions throughout the year and the recorded  $\delta^{18}\text{O}_C$ -values is called the Isotopic Transfer Function. The production of foraminifer shells largely depends on the seasonal temperature distribution (annual mean and variability [10]), but other ecological factors, such as food availability, may have to be considered as well. It will be easy to make this model very complicated, considering the number of side effects involved. Hence the ecology incorporated in our models has to be simplified.

**1.4. The Arabian Sea.** In order to test our models, we make use of data from two sediment cores collected from the Arabian Sea [3]. Core 905P is located in the upwelling area off Somalia (to be precise,  $10^\circ 46''\text{N}$  ;  $51^\circ 57''\text{E}$ ) and core 929P is located north of the island of Socotra ( $13^\circ 42''\text{N}$  ;  $53^\circ 15''\text{E}$ ). We focus on the last 30,000 years, thus covering what is known as the last Glacial-Interglacial Cycle. Three intervals can be recognised. Measuring time in units of a thousand years, a kilo-year (ky), and choosing the origin in the present, these are 1) the time span from 30–18 ky representing the conditions of the Last Glacial, 2) from 18–10 ky representing the transition from Glacial to Interglacial conditions (also known as Termination I) and, 3) the time span from 10–0 ky representing the interglacial conditions of the Holocene. In both cores the  $\delta^{18}\text{O}_C$  of three species, *G. bulloides*, *G. ruber* and *N. dutertrei*, were measured. In addition, both cores have an independent estimate

of past sea surface temperature, derived from the so-called  $U_{37}^{k'}$  ratio. It is beyond the scope of this paper to discuss this temperature proxy (an indirect measure for a variable which is not observable directly) in detail, but it is important to remember that it provides a reliable independent sea surface temperature estimate, that is based on microfossils other than planktic foraminifera (in this case coccolithophorids). The  $U_{37}^{k'}$  temperature proxy cannot be related to a certain time of the year or season, because it is poorly known when these fossils are produced most. For further information on this temperature proxy we refer to the work of Ivanova [3] and references therein.

The present research is in part aimed at obtaining a method of measuring the surface sea temperature which is independent from the  $U_{37}^{k'}$  temperature determination. Another goal is to obtain a measure for the variability of the surface sea temperature during the year.

The hydrography in the western Arabian Sea is controlled by the monsoon system. During summer (June–September) the SW (south-west) monsoon winds blow over the Arabian Sea and cause upwelling in the area off Somalia. This results in lower sea surface temperatures and higher biological productivity since cold and nutrient-rich waters are brought to the sea surface from deeper regions. In winter (December–March), the NE-monsoon winds blow from the continent to the sea and do not cause upwelling, but result in convective mixing of the upper layers of the ocean. This also causes increased biological productivity, but generally does not lower the sea surface temperature as much as during the SW-monsoon period. The inter-monsoon periods are characterised by a relatively high sea surface temperature and low biological productivity. Based on present-day observations [1], it is evident that the planktic foraminifer shells are mainly produced during the two monsoon seasons and much less during the inter-monsoon periods. Consequently, it can be expected that the fossil shells found in the sedimentary record were produced during the SW- or NE-monsoon period. It therefore makes sense to reconstruct sea surface temperatures of the two monsoon periods only.

**1.5. Secondary calcification.** The shells of planktic foraminifera are mainly composed of so-called primary calcite, a type of calcium carbonate that is formed during their life in the surface waters of the oceans. It is known, however, that shells of equal size found in and on the sediments on the sea-floor often have a higher shell mass compared to the shells found in the surface layers of the oceans. The main reason for this increase in shell mass is the formation of an extra calcite layer, also known as secondary calcite, see e.g. [5]. This crust is formed at the end of the foraminifer life cycle, at a depth in the ocean where

reproduction takes place. For “shallow dwelling” species, such as considered in this study, this depth level is found roughly between 50 and 100 meter. At these depths the water temperature is lower than the sea surface temperature, which thus results in an increase of the  $\delta^{18}\text{O}_C$  of the shell. Secondary calcite therefore may mask the  $\delta^{18}\text{O}_C$  of primary calcite. The amount of secondary calcification differs for different species: *N. dutertrei* and *G. ruber*, for example, have more secondary calcite than *G. bulloides*. This process obviously obstructs the straightforward use of the  $\delta^{18}\text{O}_C$  of fossil shells in the calculation of sea surface temperatures. In this study, we assume that the amount of secondary calcification is a constant fraction of the total shell weight, and that this fraction is species dependent. We also assume that the temperature at which the secondary calcite is formed has a constant offset from the sea surface temperature. These two assumptions allow us to correct for the effect of secondary calcification on the  $\delta^{18}\text{O}_C$  of the shells, by subtracting a constant value from each observation (section 2.2).

## 2. A simple mathematical model for the production of fossil layers

In this section two models describing how sea surface temperatures are reflected in fossil foraminifer skeletons are discussed. The simplest one takes into account the influence of temperatures only, the other one addresses the importance of food availability as well. Rather than discussing each model separately, they will be dealt with simultaneously. Both models consist of the same components, differing only in the way each component is filled in:

1. Modelling the dependence of foraminifera on environmental conditions such as sea surface temperature and food availability.
2. Modelling seasonal variations of the environmental conditions.
3. The relation between temperature and  $\delta^{18}\text{O}$ -values.
4. Prediction of the resulting measurements in fossil cores.
5. Reconstruction of paleo-temperature from the fossil core data.

The following sections mirror these parts of the models. The first component is discussed in section 2.1.1, the second in 2.1.2. Parts 3 and 4 are combined in section 2.1.3 and the reconstruction process for sea surface temperatures is finally described in section 2.1.4. The results of the analysis of the experimental data using this model are presented in section 2.2.

### 2.1. Description of the model.

2.1.1. *Dependence of foraminifera on environmental conditions.* In population dynamics many different ways exist to model the dependence of the population size of a certain species on environmental conditions.

Species $A$	$T_{\min,A}$ ( $^{\circ}C$ )	$T_{\max,A}$ ( $^{\circ}C$ )	$\bar{T}_A$ ( $^{\circ}C$ )	$\sigma_A$ ( $^{\circ}C$ )
<i>G. ruber</i>	13	32	32	14
<i>G. bulloides</i>	3	19	11	4
<i>N. dutertrei</i>	15	25	20	2.5

TABLE 1. Parameters describing the temperature dependence of the three different species. The values are taken from [13].

In general these models, of which one possible model is discussed in section 3, may lead to complicated ((quasi-)periodic, chaotic) behaviour. Even if the system simply tends to a steady state (depending on temperature), the population needs time to adjust to changing environmental conditions. In fact, the life cycle of an individual foraminifer lasts about two to four weeks, so the biological response of the whole population on a changing environment takes place on this time scale, or slower. This may well be the reason for the large amount of scatter in the data [13] showing the relation between population size and temperature. However, in this simplified model we will assume that the population adapts instantaneously and is always at its equilibrium size corresponding to the conditions present. Namely, we assume there is a direct relation between the population size and temperature given by a Gaussian distribution

$$(69) \quad P_A(T) = \alpha_A e^{-\frac{(T-\bar{T}_A)^2}{2\sigma_A^2}}$$

for species  $A$ , where  $T$  is the sea surface temperature. The temperature range  $[T_{\min,A}, T_{\max,A}]$ , the optimal temperature  $T_A$  and standard deviation  $\sigma_A$  for the three species we consider can be found in Table 1. The value of the constant factor  $\alpha_A$  depends on the exact definition and units chosen for  $P_A$  (population size, density, flux of skeletons, calcite deposited). It does not seem possible to estimate  $\alpha_A$  accurately. Fortunately, its value is not important in our analysis since this factor scales out of the calculations.

Note that all of these foraminifera die and settle on the bottom of the ocean, so we can also refer to this  $P_A(T)$  as the *production* of fossil shells of species  $A$ . The parameters tabulated in Table 1 stem from present-day measurements [13]. Although it is hard to quantify this due to the large amount of scatter, it is clear that *G. ruber* favours high temperatures, whereas *G. bulloides* prefers colder waters. The *N. dutertrei* species flourishes under moderate conditions. For each species a temperature range, optimal temperature (for which the population size is maximal) and standard deviation is estimated from the data [13]. The maximum and minimum temperatures are set to have a distance of two standard deviations from the mean. Outside the ranges  $[T_{\min,A}, T_{\max,A}]$ ,

Species $A$	$\mu_A$	$\kappa_A$	$\nu_A$	$\lambda_A$
<i>G. ruber</i>	0.4	0.03	1	0.8
<i>G. bulloides</i>	0.2	0.6	0.004	1.9
<i>N. dutertrei</i>	0.6	1.9	1.6	1.6

TABLE 2. Parameters describing the dependence of the three different species on food availability. The values are estimated from Peeters, unpublished data.

the respective species are barely present at all. We experimented with truncating the production function (69) to zero outside these temperature ranges, but this did not change the results significantly. The results in this paper are obtained by using the Gaussian formula (69) for all  $T$ .

The production function (69) describes the temperature dependence of the different species. Another important factor is the food supply. Two main sources of food can be distinguished on which the foraminifera feed, phytoplankton and zooplankton. The species *G. ruber* feeds mainly on zooplankton, *G. bulloides* feeds mainly on phytoplankton, whereas *N. dutertrei* can feed on both, making it less sensitive to the food supply. Sufficient data quantifying this are not available at the moment. For the moment, the dependence of the populations on the nutrients is modelled simply by multiplying the temperature production function (69) with a food factor, resulting in

$$(70) \quad P_A(M, N, T) = (\mu_A M^{\kappa_A} + \nu_A N^{\lambda_A}) e^{-\frac{(T-\bar{T}_A)^2}{2\sigma_A^2}}$$

where  $M$  and  $N$  denote the concentration of phyto- and zooplankton respectively ( $\text{mg}\cdot\text{m}^{-3}$ ) and  $\kappa_A$ ,  $\lambda_A$ ,  $\mu_A$  and  $\nu_A$  are coefficients describing the sensitivity of species  $A$  to the different food sources. In this study we use the values shown in Table 2 for the parameters  $\kappa_A$ ,  $\lambda_A$ ,  $\mu_A$  and  $\nu_A$ . They are rough estimates from experimental data.

A note of caution with regard to the production function (70): to our knowledge it has not yet been attempted to describe the abundance of foraminifera in terms of temperature and food availability, and it may be possible to improve upon (70) on the basis of further research. For instance, the data show a correlation between the abundance of the foraminifera and the phosphate concentration (which is the main food source for phytoplankton) and total biomass (essentially the sum of phyto- and zooplankton).

We conclude this section about the behaviour of the foraminifera under different circumstances by summarising our main assumptions: the populations are always in steady state and adapt to changes in environmental conditions instantaneously (a so-called “quasi-steady” model);

either the population density does not depend on food availability and the production function (69) is used or the population density is influenced by two different food sources and a food factor is included, see equation (70).

2.1.2. *Modelling the environmental conditions.* This section deals with the way we model the seasonal variation of sea surface temperature and food availability, namely we will consider temperature and food availability as a function of time throughout the year.

In the introduction it was described already that the Arabian Sea, for which this model is considered, is strongly influenced by the monsoon system. It thus makes sense to divide the year into two distinct seasons, the SW-monsoon period in the summer and the NE-monsoon period in the winter. A simple temperature model can be constructed by assuming a constant temperature in each season. We fix the duration of each monsoon season at four months. During the inter-monsoon periods, the abundance of the foraminifera is very low due to the lack of food. Therefore we will neglect the production of fossils during those periods. The SW-monsoon is stronger than the NE-monsoon, hence the upwelling induces lower sea surface temperature in the summer whereas the winter temperature is higher. This is illustrated in Figure 2; notice that  $T_{NE}$  and  $T_{SW}$  are not chosen a priori but will be deduced from the data. Moreover, we interpret (69) to be valid during the two monsoon periods while the production  $P_A(T) = 0$  in between the monsoons due to lack of nutrients (hence the temperature in the inter-monsoon periods is (left) unspecified). Also, only the ratio of the duration of the SW- and NE-monsoon is relevant for the outcome of the model.

In principle, alternative temperature models are also possible, e.g. [9]. But we have one restriction: for our procedure to work a temperature curve should be completely described by no more than two parameters. For example, a sinusoidal cycle with a mean temperature and an amplitude could be specified as well. The temperature curve used in section 3 (equation (80)) also depends on two parameters. Here we remark only that this is connected with the fact that we have data on three species. If we consider  $k$  species we can allow temperature to depend on  $k - 1$  parameters. The reason for this is discussed in more detail in section 2.1.4. Although the model can be used with other descriptions of the yearly temperature cycle as well, the calculations are simplified considerably by assuming two seasons of constant temperature. We therefore limit ourselves to this description in the current

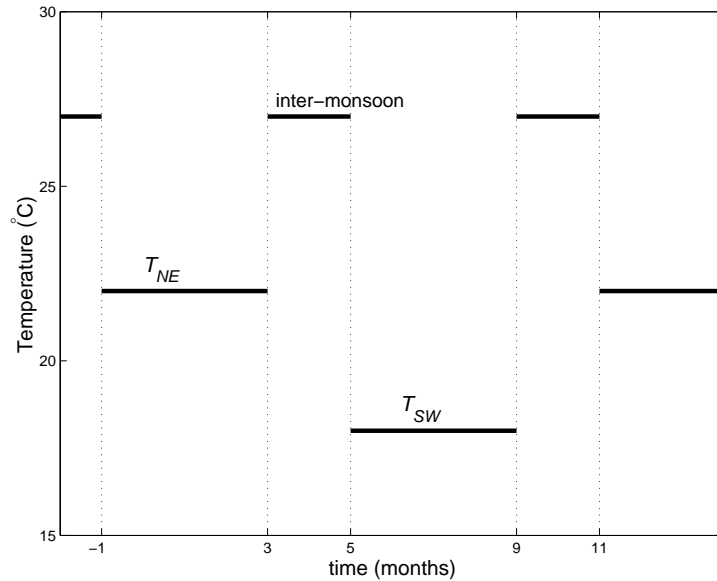


FIGURE 2. The description of the yearly signal of sea surface temperature in the Arabian Sea; two monsoon-seasons at constant temperature, the SW-monsoon during summer and the NE-monsoon during winter.

section:

$$(71) \quad \begin{aligned} T &= T_{SW}, && \text{during the SW-monsoon (summer),} \\ T &= T_{NE}, && \text{during the NE-monsoon (winter),} \\ T &= \text{unspecified,} && \text{during the inter-monsoon periods.} \end{aligned}$$

Having described the temperature dependence on time, the environmental conditions are sufficiently specified for the simplest model (69) in which temperature only is considered. For model (70) we need to specify time dependence of the food availability as well.

An accurate description of the food supply is much harder because phyto- and zooplankton have complicated dynamics of their own, see [7]. In fact, the phytoplankton consumes inorganic nutrients, like phosphate, which are brought to the sea surface during an upwelling phase. Zooplankton feeds, though not exclusively, on phytoplankton. Therefore its bloom occurs only after the phytoplankton population has begun to develop. We will not try to model this here. In order to investigate the influence of the food availability on recorded  $\delta^{18}\text{O}$ -values we simply try to specify the values of  $M$  and  $N$  through time, like we did for the temperature. Note that the two-dimensional food availability function  $(M(t), N(t))$  should depend on at most two parameters, so each of the

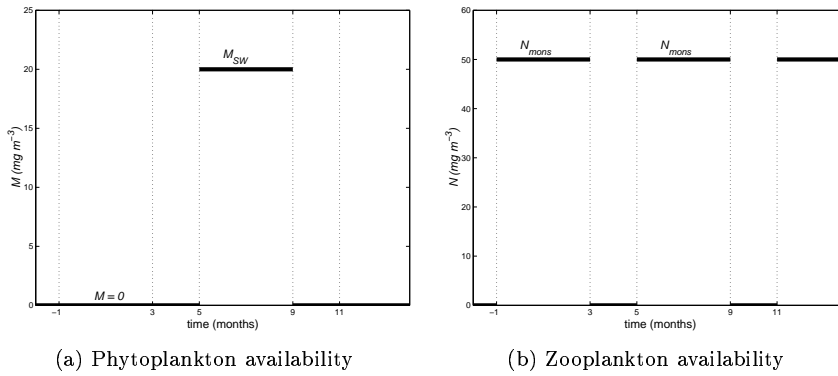


FIGURE 3. Description of the yearly cycle of food availability for the foraminifera: (a) The phytoplankton is assumed to be present only during the SW-monsoon (summer). (b) The zooplankton is assumed to be equally available during all seasons.

components  $M(t)$  and  $N(t)$  may depend on one parameter only. To simplify the calculations we use the same two seasons as before, assuming that the phytoplankton is present in the summer season only, whereas the zooplankton is present the whole year round (Fig. 3). This is based on field observations showing that the abundance of phytoplankton is much lower during the winter monsoon than during the summer monsoon period.

This concludes the modelling of the environmental conditions. For the model without nutrients, only the temperature dependence (71) (Figure 2) is used. The other model uses the same temperature model and incorporates the food availability description as in Figure 3:

$$(72) \quad \begin{aligned} M &= M_{SW}, & N &= N_{mons} & \text{during the SW-monsoon (summer),} \\ M &= 0, & N &= N_{mons} & \text{during the NE-monsoon (winter),} \\ M, N &= 0, & & & \text{during the inter-monsoon periods.} \end{aligned}$$

2.1.3. *The resulting core data.* This section deals with the main ingredient of the model: how do the previous two sections relate to the data we measure in the cores? Two aspects of foraminifera skeletons are measured in the cores, the relative abundances of the different species and the mean  $\delta^{18}\text{O}$ -values for each species. In principle it is possible to obtain absolute fluxes for each species instead of relative abundances by measuring the amount of deposited skeletons per period of time. However, these absolute fluxes are less reliable because to determine them

one also needs to estimate the age of the core (for example by radioactive carbon measurements). Therefore, relative abundances are more commonly used to express the results of measurements.

In our model the production functions  $P_A$  from equations (69) or (70) describe the number of skeletons that settle on the bottom of the ocean. The total production of one species during a year will be the integral of  $P_A$  over this period. In the cores, separate years, let alone separate seasons, can not be distinguished. So the measurements in the core show averaged productions over several years. From the model the relative abundances are found by dividing the yearly production of one species by the total production of all species together. This leads to

$$(73) \quad \chi_A = \frac{\int P_A(M(t), N(t), T(t)) dt}{\int (P_{rub} + P_{bul} + P_{dut}) dt}$$

for the relative abundance of species  $A$ , with the obvious need to suppress  $M(t)$  and  $N(t)$  from the notation if (69) is used.

Moreover, the  $\delta^{18}\text{O}_C$ -values of the fossil foraminifera can be measured. As was explained in section 1.2, the oxygen isotope composition in their skeleton reflects the temperature at which they lived, according to formula (68). It can be measured in the core as well, for each species separately. Because it is not possible to measure it for a single foraminifer, only averaged values over several years can be recovered. This average  $\delta^{18}\text{O}_C$ -value is weighed by the number of skeletons produced in different periods (and hence reflects the conditions under which the respective species flourishes). This average for species  $A$  reads

$$(74) \quad \overline{\delta^{18}\text{O}_A} = \frac{\int \delta^{18}\text{O}_A(T(t), \delta^{18}\text{O}_W) P_A(M(t), N(t), T(t)) dt}{\int P_A(M(t), N(t), T(t)) dt}$$

again with the obvious change of notation if (69) is used. Because  $\delta^{18}\text{O}_W$  appears in equation (68) in a linear way, it can be pulled out of the averaging. Hence

$$(75) \quad \begin{aligned} \overline{\delta^{18}\text{O}_A} &= \langle \delta^{18}\text{O}_A(T(t), \delta^{18}\text{O}_W) \rangle_A \\ &= \langle f(T) \rangle_A + \langle \delta^{18}\text{O}_W \rangle_A \\ &= \langle f(T) \rangle_A + \delta^{18}\text{O}_W \end{aligned}$$

where we define the (species dependent) averaging  $\langle \cdot \rangle_A$  abbreviating the integrals and

$$(76) \quad f(T) = 25.778 - 3.333 \cdot (43.704 + T)^{0.5}.$$

Note that we incorporated the correction for the vital effect  $\delta^{18}\text{O}_{VE}$  in  $\delta^{18}\text{O}_A$  without a change in notation. This will be done throughout the remainder of this section, except in Figure 4. The final equality is

based on the fact that  $\delta^{18}\text{O}_W$  does not change much over years so we can assume that it was the same in all seasons.

2.1.4. *Reconstruction of sea surface temperatures.* Equations (73) and (75) predict the outcome of core measurements according to our models. In this section all ingredients of the two models discussed in sections 2.1.1 to 2.1.3 are put together. By working out the equations (73) and (75), we find the Isotopic Transfer Function, i.e. the influence of the environmental conditions on the oxygen isotope composition and the relative abundances.

First consider equation (75). It contains the unknown background value  $\delta^{18}\text{O}_W$ , which is the same for all species. Therefore the  $\delta^{18}\text{O}_W$ -value can be eliminated by subtracting the  $\delta^{18}\text{O}$ -values of two species. For the three species *G. ruber*, *G. bulloides* and *N. dutertrei* this leads to two independent differences

$$(77) \quad \begin{aligned} \frac{\overline{\delta^{18}\text{O}_{bul}} - \overline{\delta^{18}\text{O}_{dut}}}{\overline{\delta^{18}\text{O}_{bul}} - \overline{\delta^{18}\text{O}_{rub}}} &= \langle f(T) \rangle_{bul} - \langle f(T) \rangle_{dut}, \\ \overline{\delta^{18}\text{O}_{bul}} - \overline{\delta^{18}\text{O}_{rub}} &= \langle f(T) \rangle_{bul} - \langle f(T) \rangle_{rub}. \end{aligned}$$

The right-hand sides of (77) depend on  $T_{SW}$ ,  $T_{NE}$ ,  $M_{SW}$  and  $N_{mons}$ . The left-hand sides of (77) can be found from the core measurements. Hence this provides us with two equations for  $T_{SW}$ ,  $T_{NE}$ ,  $M_{SW}$  and  $N_{mons}$ .

The three relative abundances sum up to one ( $\chi_{rub} + \chi_{bul} + \chi_{dut} = 1$ ), so only two of them are independent. Hence, when we fit the outcome of the model to the measured relative abundances we have again two independent equations. This implies that if only  $\delta^{18}\text{O}$ -values are used the maximum number of independent parameters that can be recovered is two, while if relative abundances are taken into account as well, four independent parameters can be determined. This is the reason why relative abundances have to be considered as well when using model (70), incorporating the influence of two types of food sources and why no more than a single parameter per food source could be used in section 2.1.2.

Working out the model without food availability leads to

$$\langle f(T) \rangle_A = \frac{\frac{4}{12}f(T_{SW})e^{-(T_{SW}-\bar{T}_A)^2/2\sigma_A^2} + \frac{4}{12}f(T_{NE})e^{-(T_{NE}-\bar{T}_A)^2/2\sigma_A^2}}{\frac{4}{12}e^{-(T_{SW}-\bar{T}_A)^2/2\sigma_A^2} + \frac{4}{12}e^{-(T_{NE}-\bar{T}_A)^2/2\sigma_A^2}}$$

for species *A*. The integrals have been evaluated easily because we assumed two seasons of constant temperature. The parameters  $\bar{T}_A$  and  $\sigma_A$  of the Gaussian temperature distribution are taken from Table 1, the factor  $\alpha_A$  from equation (69) drops out and  $f(T)$  is given by equation (76). The two unknowns are  $T_{SW}$  and  $T_{NE}$ , which of course are the same for each species. Hence substituting this in equation (77) leads to

two equations for two unknowns. They must be solved numerically in order to obtain  $T_{SW}$  and  $T_{NE}$  from the measured  $\delta^{18}\text{O}$ -differences.

The equations for the model incorporating the effect of food availability are more elaborate. The integrals simplify again due to the assumption of two seasons with constant environmental conditions. There are four unknowns,  $T_{SW}$ ,  $T_{NE}$ ,  $M_{SW}$  and  $N_{mons}$ . Four equations are obtained by considering the relative abundances (73) as well, for two species. It will come as no surprise that these equations (77) and (73) have to be dealt with numerically as well.

We implemented these equations in *Mathematica* and in MATLAB, the latter appearing faster and more robust. The results are discussed in section 2.2. Note that, for reasons of numerical robustness, we did not use standard root finding routines to solve equations (77) and (73). Instead, we used a least squares method: we have taken the differences between left- and right-hand sides of the system of equations (77) and (73) and considered the sum of squares of these differences. The resulting function was minimised with respect to the variables to be solved for:  $T_{SW}$ ,  $T_{NE}$ ,  $M_{SW}$  and  $N_{mons}$ . Of course, if the system has a solution, the minimum is zero.

Finally, note that in principle it is possible to work out the model with other temporal behaviour of the environmental conditions. The resulting integrals will be more difficult to evaluate and have to be calculated numerically as well. However, as long as the number of parameters describing them equals the number of equations, it will generally be possible to recover them in the same manner as described above.

**2.2. Results of the simple model.** In this section the results of the models are discussed. As input data from two cores are used, core 905P and core 929P, see section 1.4. The  $\delta^{18}\text{O}_C$ -values measured for the three different species *G. bulloides*, *N. dutertrei* and *G. ruber* are shown in Figure 4(a) and 4(b).

A striking aspect in these figures is the clear decrease in  $\delta^{18}\text{O}_C$ -values at the transition between the glacial and interglacial period, around 15 thousand years ago. First this was interpreted as the result of increasing temperature, but it appeared to be strongly influenced by the change in the background value  $\delta^{18}\text{O}_W$ , see equation (68). The melting of polar ice-sheets caused  $\delta^{18}\text{O}_W$  to decrease significantly.

Another aspect is that although the difference between the different species is partly due to the vital effect  $\delta^{18}\text{O}_{VE}$ , differences between the species remain present after correcting for it. We precisely aim to describe these differences with our models.

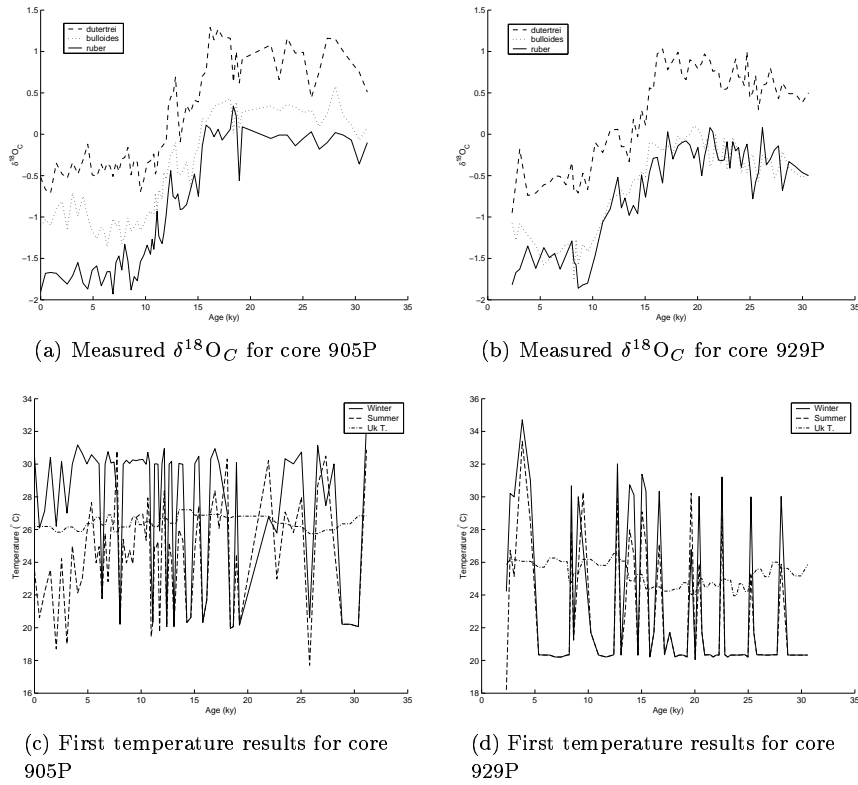


FIGURE 4. The raw  $\delta^{18}O_C$ -data after [3] for (a) core 905P and (b) core 929P, and the resulting temperatures for model (69) without food availability for (c) core 905P and (d) core 929P.

The first results using the model (69) without food availability, are shown in Figure 4(c) and 4(d). As an independent reference  $U_{37}^{k'}$ -temperature (see section 1.4) is shown as well. These results should be rated as unreliable. It is highly unlikely that such sudden and vigorous variations in summer and winter temperature have occurred. The changes in summer and winter temperature are expected to be comparable to the changes of the  $U_{37}^{k'}$ -temperature. Moreover, there seems to be a preference for a temperature of about  $20.5^\circ C$ , with exactly coinciding summer and winter temperatures, hence no temperature variation. If there would be no temperature variation during the year, all species would have recorded the same temperature, hence the same  $\delta^{18}O$  (after correction for vital effect). This is not consistent with the data, which do show differences between species. The reason for these inconceivable results is illustrated in Figure 5(a); the measured  $\delta^{18}O$ -differences lie outside the range that can be explained by our model. The problem is

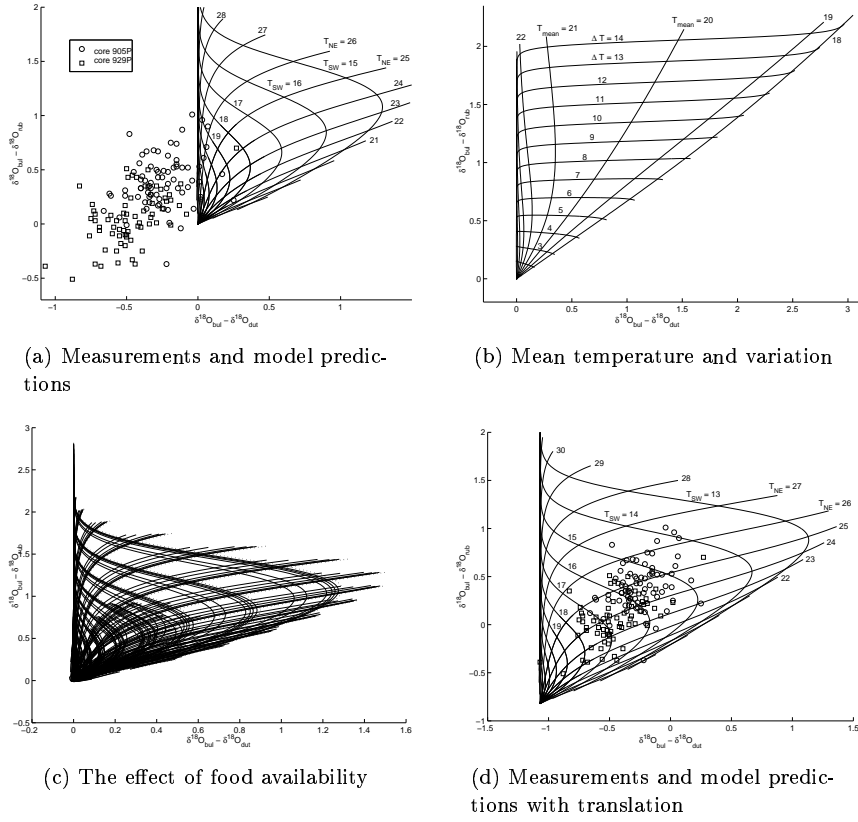


FIGURE 5. Space of  $\delta^{18}\text{O}$ -differences, corrected for Vital Effect. The measurements from core 905P are indicated by circles, from core 929P by squares. (a) shows the measurements and model predictions for temperatures  $T_{NE}$  ranging from 15–25 °C,  $T_{SW}$  from 18–35 °C. (b) shows the same model predictions but as a function of mean temperature from 18–26 °C and seasonal difference from 0–14 °C. (c) shows the influence of food availability showing the same as (a) for  $M_{SW} = 10, 20, 50, 10, 20, 50$  and  $N_{mean} = 20, 20, 50, 50, 50, 100$  respectively. (d) shows the same as (a) with a translation (attributed to secondary calcification) by which all measurements are within the range of the model predictions.

that the data suggest that *G. ruber* and *N. dutertrei* record a lower temperature in their oxygen isotope compositions than *G. bulloides*, whereas in our model the optimal temperature  $\bar{T}_{bul}$  is smaller than both  $\bar{T}_{rub}$  and  $\bar{T}_{dut}$ .

Figure 5(a) shows the space of  $\delta^{18}\text{O}$ -differences. The lines show the model results where the temperature of one of the seasons is fixed. The same model results are shown in Figure 5(b) with lines of constant mean temperature  $T_{mean} = \frac{1}{2}(T_{SW} + T_{NE})$  and variation  $\Delta T = T_{NE} - T_{SW}$ . From these figures it would be possible to read the temperatures responsible for certain core measurements. A measurement on the intersection of two lines would, according to the model, have been produced by the corresponding temperatures. The lines for constant variation  $\Delta T$  are almost horizontal. This means that the temperature variation is recorded mainly by the vertical difference  $\delta^{18}\text{O}_{bul} - \delta^{18}\text{O}_{rub}$  with only a moderate correction for mean temperature, confer [11]. The  $\delta^{18}\text{O}$ -differences do not depend on mean temperature much, except in the range 19–21 °C, which is around the optimal temperature of *N. dutertrei*.

The fact that most measurements are not within the range of the model explains the bad results that were shown in Figure 4(c) and 4(d). In particular the points where the temperatures  $T_{SW}$  and  $T_{NE}$  were found to be equal, is related to this and with our use of least squares: the origin (0,0) without difference between species is an extreme point and is the closest the model can get to many of the measurements.

We propose to expand the model to be able to explain the observed measurements. Let us see what happens when we include food availability in the model. This might cause the production patterns to be changed such that they record other temperatures than was to be expected when temperature only would play a role. However, this seems to be of minor influence. In order to illustrate this, Figure 5(c) shows the model predictions for  $\delta^{18}\text{O}$ -differences under several conditions. In fact, the same temperature ranges  $T_{SW} = 15\text{--}25^\circ\text{C}$ ,  $T_{NE} = 18\text{--}35^\circ\text{C}$  as in Figure 5(a) are shown for six different values for the food parameters:  $(M_{SW}, N_{mean}) = (10, 20), (20, 20), (50, 50), (10, 50), (20, 50)$  and  $(50, 100)$ . Dotted lines showing the predictions without food availability are also included. This figure is barely readable, but the important thing which should be noted from Figure 5(c) is that the region of possible  $\delta^{18}\text{O}$ -differences covered by the model is hardly enlarged by the incorporation of food availability. Although the inclusion of food availability in the model is at present fairly rudimentary and could be made more sophisticated, the first indications are that the nutrients do not solve the problem!

Another explanation for the difference between our model results and the measurements is the fact that secondary calcification may occur, as is explained in the introduction, section 1.5. The model described so far, predicts the  $\delta^{18}\text{O}_C$ -value of shells that are free of secondary calcite. At the end of their life cycle, they settle down on the bottom of the ocean.

In this period their oxygen isotope composition will increase due to secondary calcification. Therefore, the  $\delta^{18}\text{O}$ -differences differ from the ones predicted by our model. To compensate for this, quantification of the process of secondary calcification for each species is necessary. Although accurate data are not available yet, a rough estimate of the correction terms needed is in the order of 0.5–1.0‰ for *G. ruber* and about 1‰ for *N. dutertrei*. The species *G. bulloides* however hardly experiences secondary calcification, so it can be expected that no correction term is needed for this species.

Comparing the model predictions to the observed measurements, Figure 5(a), we found that a minimum correction of 1.07‰ for the difference  $\delta^{18}\text{O}_{bul} - \delta^{18}\text{O}_{dut}$  and 0.82‰ for  $\delta^{18}\text{O}_{bul} - \delta^{18}\text{O}_{rub}$  is needed to ensure that all measurements are contained within the region of model predictions. These values compare well to the roughly estimated values. Because it is complicated to quantify the effect of secondary calcification with great accuracy, we will use these pragmatic correction terms for now. The result is shown in Figure 5(d). Of course, all measurements can be reached by the model now. The results for the model after correcting for secondary calcification are shown in Figure 6, for core 905P in the left column, for core 929P in the right one. The upper two plots 6(a) and 6(b) contain the results using model (69), including temperature effects only. Figure 6(c) and 6(d) show the results using model (70), incorporating food availability as well. In that case, we also solve for the parameters describing the food sources,  $M_{SW}$  and  $N_{mean}$ , which are shown in the lower two figures. For three measurements in core 929P the routine searching for the least squares minimum failed to converge. These points are marked by stars in Figure 6(d). Though marked as suspect, they do not seem to be very different from the other points.

The results shown in Figure 6 are much more plausible than those in Figure 4. The summer and winter temperatures  $T_{SW}$  and  $T_{NE}$  change a few degrees only and rapid oscillations as in Figure 4 do not occur. This is what should be expected. The results show an increase in seasonal variability from the glacial to the interglacial (present) period. This can be explained by the fact that there are indications that upwelling has increased in this period. This causes the sea surface temperature to be lower during the SW-monsoon, in the summer, because of enhanced upwelling. Moreover, the solar radiation is higher during the interglacial period. Therefore the temperature in the NE-monsoon period has increased. Both effects are clearly visible in core 905P. Core 929P is taken

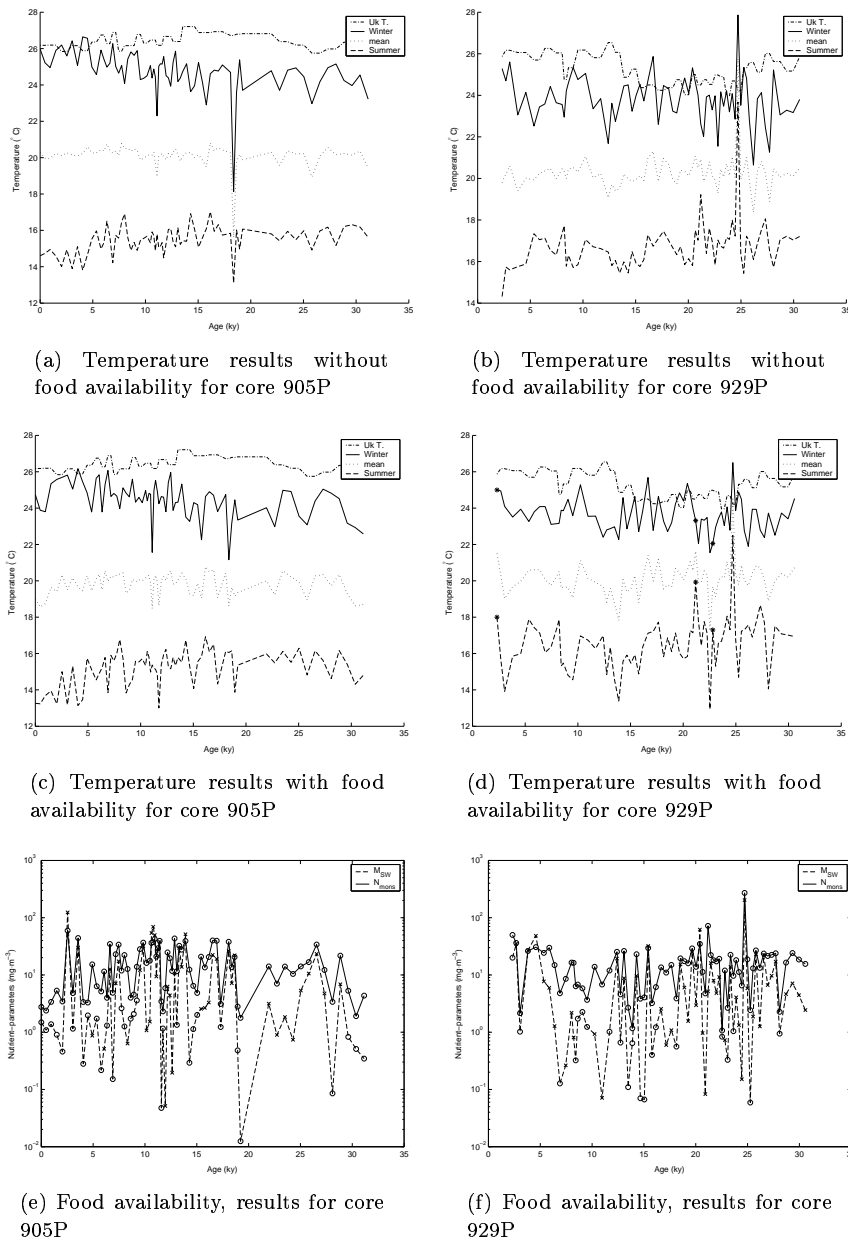


FIGURE 6. Results of the models after correcting for secondary calcification by a translation. The recovered sea surface temperatures using model (69), without food availability, are shown in (a) for core 905P and in (b) for core 929P. The temperatures using model (70), with food availability included, are shown in (c) for core 905P and in (d) for core 929P. The corresponding concentrations of phyto- and zooplankton are shown in (e) for core 905P and in (f) for core 929P.

at a different spot in the Arabian Sea, where upwelling is less important. Cold water reaches this spot by advection from other regions. As a result, the decrease in SW-monsoon temperature is less pronounced.

For both cores the sea surface temperatures we find are lower than  $U_{37}^{k'}$ -temperatures. There may be several explanations for this. Foraminifera live at about 30 m depth, hence in a colder environment than immediately at the surface where  $U_{37}^{k'}$ -temperature is recorded. According to [11] about 1.3–1.7 °C should be added to the temperatures recorded by foraminifera. In that case, the  $U_{37}^{k'}$ -temperatures would be included in the yearly temperature range calculated through our model. Another explanation might be that the coccolithophorids—the microfossils used for  $U_{37}^{k'}$ -temperature—live in another season. If their ecological preference would be during the inter-monsoon period, they would certainly record higher temperatures than the foraminifera, which live mainly during the monsoon periods. Finally, it may well be necessary to improve our implementation of secondary calcification.

The sharp decrease in (winter) temperature in Figure 6(a) about 18 ky ago is diminished considerably in Figure 6(c). Apparently, this peak can be attributed to a nutrient effect not taken into account in Figure 6(a). The positive peak in both winter and summer temperature at about 25 ky ago in core 929P probably is an outlier.

The results in Figure 6(e) and 6(f) are fairly consistent with present-day measurements, which show the concentration of phytoplankton  $M$  to vary between 2–60 mg·m<sup>-3</sup> whereas the concentration of zooplankton  $N$  is somewhat higher between 9–90 mg·m<sup>-3</sup>. The model results show  $N_{mean}$  to be larger than  $M_{SW}$  as well.

Although the absolute value of  $M_{SW}$  and  $N_{mean}$  seems to be quite plausible, there is one aspect which should make the results in the figures 6(c), 6(d), 6(e) and 6(f) completely unreliable. The crosses in Figure 6(e) and 6(f) indicate that the corresponding value for  $M_{SW}$  found by the model is negative (the plot shows its absolute value)! This is clearly problematic from the biological point of view and demonstrates that the model should be investigated further before we can draw conclusions from it. Finally, a quick glance at Figure 6 suggests that there is a correlation between the  $U_{37}^{k'}$ -temperature and the temperature  $T_{SW}$  during the SW-monsoon season. This needs further investigation as well.

### 3. A population dynamics model

The reconstruction of the sea surface temperature has so far been based on the assumption that the population adapts instantaneously to the changes in its environment. In this section we take a different

approach and formulate a dynamic model consisting of a system of ordinary differential equations (ODEs) describing the populations of the three types of foraminifera and their food sources. Such an ODE model is very flexible and can easily be amended to include many different phenomena if desired. Here we restrict to the effects caused by changes in temperature and food availability.

In particular, during the southwest monsoon there is a strong growth in the populations of the foraminifera (and a corresponding increase in the flux of foraminifera shells to the sea floor [1]). This growth is caused by the upwelling of cold nutrient-rich water near the coast. The flux of some species depends strongly on the availability of these nutrients, while other species seem to respond mainly to the temperature variation. This information can be used to obtain a more detailed picture of the life cycle of the foraminifera.

The objective is to construct a population dynamics model for the various species of foraminifera and food sources. As is known in case of one single food source, there will be a survival of the fittest so that only one species will remain after some time (“competitive exclusion”, see e.g. [12]). It is therefore crucial that the model encompasses at least two different food sources for the populations. We propose a population model for the three species *G. ruber* ( $R$ ), *G. bulloides* ( $B$ ), and *N. dutertrei* ( $D$ ), feeding on two food sources (phyto- and zooplankton) which we call  $M$  and  $N$  as before. The aim of the model is to see what the effect of the upwelling during the southwest monsoon can be. As mentioned before, the ODE model also provides the opportunity to analyse the influence of additional effects, such as the northeast monsoon, the role of plankton as a primary food source or external effects such as the moon cycle.

We give here the simplest model with only growth and death terms for the populations  $R$ ,  $B$  and  $D$  and their food sources  $M$  and  $N$ . We assume that  $R$  and  $D$  feed off  $N$ , while  $B$  and  $D$  live off  $M$  (see section 2.1.1). The growth of the species is determined by availability of food, by the carrying capacity of the species, and by the preferred temperature. We assume, as before, that each species has a preferred temperature, denoted  $\bar{T}_R$  for *G. ruber*, and a corresponding spread in temperature modelled by a standard deviation  $\sigma_R$ . The growth term of the food sources  $N$  and  $M$  is dominated by the upwelling, and we will model this as a function of the temperature change. We denote the growth functions by  $G_M$  and  $G_N$  for the moment and choose a specific

function later. The ODE model then reads:

$$\begin{aligned}
\dot{R} &= \alpha_R N \ell(R) \frac{1}{\sigma_R} e^{-(T-\bar{T}_R)^2/2\sigma_R^2} - \beta_R R, \\
\dot{B} &= \alpha_B M \ell(B) \frac{1}{\sigma_B} e^{-(T-\bar{T}_B)^2/2\sigma_B^2} - \beta_B B, \\
\dot{D} &= \frac{1}{2}(\alpha_{DM} M + \alpha_{DN} N) \ell(D) \frac{1}{\sigma_D} e^{-(T-\bar{T}_D)^2/2\sigma_D^2} - \beta_D D, \\
\dot{M} &= G_M(\dot{T}) - \mu_B M \ell(B) \frac{1}{\sigma_B} e^{-(T-\bar{T}_B)^2/2\sigma_B^2} \\
&\quad - \mu_{DM} M \ell(D) \frac{1}{\sigma_D} e^{-(T-\bar{T}_D)^2/2\sigma_D^2}, \\
\dot{N} &= G_N(\dot{T}) - \mu_R N \ell(R) \frac{1}{\sigma_R} e^{-(T-\bar{T}_R)^2/2\sigma_R^2} \\
&\quad - \mu_{DN} N \ell(D) \frac{1}{\sigma_D} e^{-(T-\bar{T}_D)^2/2\sigma_D^2}.
\end{aligned}
\tag{78}$$

The function  $\ell$  in this model is usually assumed to be a simple linear term  $\ell(R) = R$ , or logistic  $\ell(R) = R(k - R)$ , but in order to control the population without restraining it entirely, we have chosen  $\ell(R) = \frac{R}{1+R/k_R}$  with  $k_R$  the carrying capacity.

The model contains a large number of parameters, but some of the parameters can be scaled out while for others a typical physical value can be chosen. Since the life cycle of the populations is around 4 weeks, we choose all the  $\beta$ -values to be equal,  $\beta = 13$  (since our unit of time is a year and 4 weeks is roughly one thirteenth of a year). The population of *G. bulloides* is around four times as large as that of *G. ruber* as well as *N. dutertrei*, under similar circumstances, so we choose  $\alpha_R = \alpha_{DN}$  and  $\alpha_B = 4\alpha_{DM}$ . The data for the preferred temperatures and the sensitivities to the temperature are known from experiments, see the columns  $\bar{T}$  and  $\sigma$  in Table 3. So now when scaling  $R$  with  $\mu_R$ ,  $B$  with  $\mu_B$ ,  $D$  with  $\mu_{DN}$ ,  $M$  with  $\alpha_{DM}$ ,  $N$  with  $\alpha_{DN}$ , then this reduces the model to the following scaled version:

$$\begin{aligned}
\dot{R} &= N \ell(R) \frac{1}{\sigma_R} e^{-(T-\bar{T}_R)^2/2\sigma_R^2} - \beta R, \\
\dot{B} &= 4M \ell(B) \frac{1}{\sigma_B} e^{-(T-\bar{T}_B)^2/2\sigma_B^2} - \beta B, \\
\dot{D} &= \frac{1}{2}(M + N) \ell(D) \frac{1}{\sigma_D} e^{-(T-\bar{T}_D)^2/2\sigma_D^2} - \beta D, \\
\dot{M} &= G_M(T) - M \ell(B) \frac{1}{\sigma_B} e^{-(T-\bar{T}_B)^2/2\sigma_B^2} - \tilde{\mu} M \ell(D) \frac{1}{\sigma_D} e^{-(T-\bar{T}_D)^2/2\sigma_D^2}, \\
\dot{N} &= G_N(T) - N \ell(R) \frac{1}{\sigma_R} e^{-(T-\bar{T}_R)^2/2\sigma_R^2} - N \ell(D) \frac{1}{\sigma_D} e^{-(T-\bar{T}_D)^2/2\sigma_D^2}.
\end{aligned}
\tag{79}$$

Here  $\tilde{\mu} = \frac{\mu_{DM}}{\mu_{DN}}$  and the new carrying capacities are scaled by the corresponding  $\mu$ -values.

Now the only terms that need to be specified are the temperature and the nutrient increase due to the upwelling. We couple this nutrient increase directly to a rise in food availability (because the inorganic nutrients are consumed by the plankton). Since the upwelling causes a decrease of the sea surface temperature, we choose to simplify the modelling of the upwelling by specifying a temperature profile and by

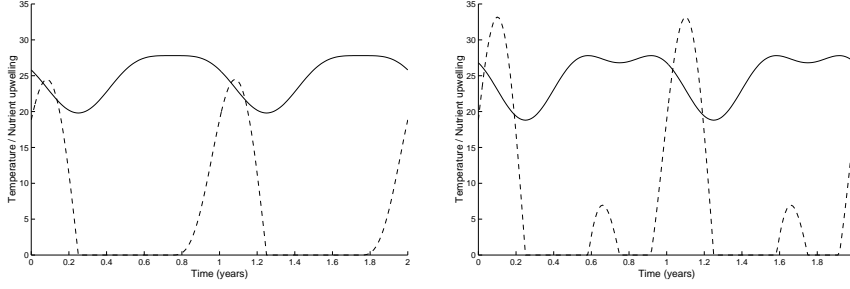


FIGURE 7. Temperature profile and nutrient upwelling for  $\gamma = 0.5$  (left) and  $\gamma = 1$ . In both graphs  $T_0 = 24.8^\circ C$  and  $T_h = 4^\circ C$ .

making the nutrient growth a function of temperature decrease only. To be specific, we take

$$\begin{aligned}
 (80) \quad G_N(T) &= -\nu_N H(-\dot{T}) \dot{T} \\
 G_M(T) &= -\nu_M H(-\dot{T}) \dot{T} \\
 T(t) &= T_0 + \frac{T_h \gamma}{2} - T_h \sin 2\pi t (1 + \gamma \sin 2\pi t)
 \end{aligned}$$

with  $H$  the Heaviside function, ensuring that only temperature decrease is related to changes in the nutrients while temperature increase has no effect. The parameter  $\gamma$  is a measure for the relevance of the northeast monsoon. Its effect on the nutrient growth is shown in Figure 7.

We study the behaviour of the populations and try to find the mean temperature  $T_0$  and the temperature variation  $T_h$  by matching the results from the ODE model with the data from the oxygen isotope compositions. The remaining parameters in the model are the three carrying capacities  $k$ , the value of  $\tilde{\mu}$  (which we arbitrarily fix at 1) and the food growth parameters  $\nu_N$  and  $\nu_M$  (the coupling constants between nutrient upwelling and plankton increase in (80)). We describe various test results in the next section.

The sensitivities  $\sigma$  to the temperature can be obtained from measurements on their temperature ranges, see Table 3. The values of the other parameters are much harder to determine. Therefore we will follow a different approach. We will set these parameters in such a way that the model (79) and (80) describes the measurements of the current foraminifera levels as accurately as possible.

**3.1. Dynamics.** We are looking for solutions to (79) that are periodic with a period of one year. This means that we can derive all relevant quantities from this solution by integration over one year.

A priori one cannot expect that the system converges to such a periodic solution. However from the numerical simulations we performed it becomes clear that for most parameter values there exist a periodic

Species $A$	$T_{\min}$ ( $^{\circ}C$ )	$T_{\max}$ ( $^{\circ}C$ )	$\bar{T}_A$ ( $^{\circ}C$ )	$\sigma_A$ ( $^{\circ}C$ )
<i>G. ruber</i>	15	30	25	2
<i>G. bulloides</i>	0	24	12	6
<i>N. dutertrei</i>	15	23	20	2.5

TABLE 3. Parameters describing the temperature dependence of the three different species under consideration. We note that these values are slightly different from those in Table 1 due to an a posteriori change in the value of the constants, a typical phenomenon for a studygroup problem indeed.

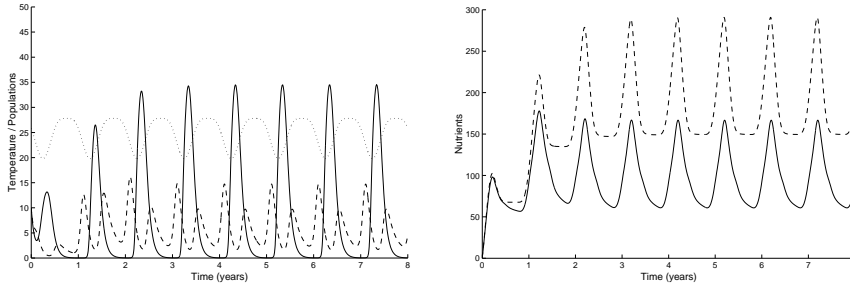


FIGURE 8. The convergence of the system towards a periodic solution, starting with arbitrary initial conditions. The left graph shows the population of *N. dutertrei* (solid) and of *G. ruber* (dashed). The dotted line shows the temperature profile. The graph on the right shows the food sources  $M$  (dashed) and  $N$  (solid) in the same simulation. Parameters:  $\bar{T}_A$  and  $\sigma_A$  as in Table 3,  $k = 10$ ,  $\nu_N = 20$ ,  $\nu_M = 20$ . Initial values:  $N = M = 1$ ,  $R = B = D = 10$ .

solution to (79). Furthermore the convergence towards this periodic solution is in general quite fast, see Figure 8. Note that in that simulation we started with initial conditions far from the final periodic solution.

We assume that the climate only changes over long periods. Over the relatively short period of the simulations there will be small variations in the climate. These variations however average out, so we will take the a fixed yearly temperature cycle. We remark that the fast convergence to the periodic solution means that the system adapts almost instantly to the changes in the climate.

Apart from the periodicity of the solution, we impose just one other condition which is derived from the present-day situation. Under the current climatological conditions ( $T_0 = 24.8^{\circ}C$ ,  $T_h = 4^{\circ}C$ ) we know that all three species are present. Therefore we adapt the food growth parameters  $\nu$  in such a way that for this temperature profile, the three species coexist. This leads to the choice  $\nu_N = \nu_M = 20$ .

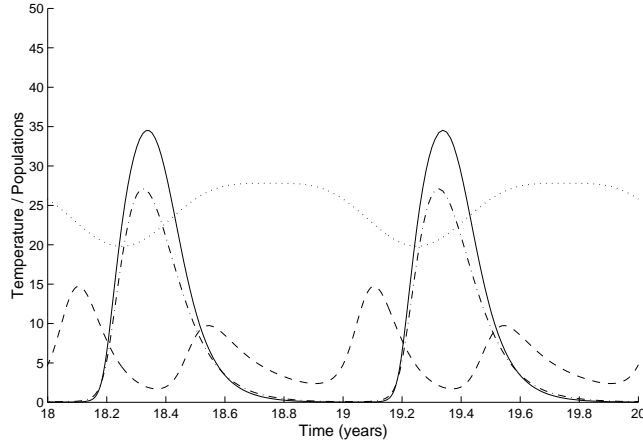


FIGURE 9. The final populations of *N. dutertrei* (solid), of *G. ruber* (dashed) and of *G. bulloides* (dash-dot) of the simulation in Figure 8. The dotted line shows the temperature profile.

In Figure 9 we see that the three species react in different ways to the environmental conditions: *G. bulloides* and *N. dutertrei* have a single growth peak during the SW monsoon when the temperature is closest to their preferred temperatures. On the other hand the preferred temperature of *G. ruber* is met twice halfway the transition between the two monsoon periods. Therefore this species has two periods of growth. The second peak is smaller because there is less food available.

**3.2. Getting temperature information from the model.** During its life the plankton records the temperature of the surrounding sea water in its shell. We can find the average temperature that is recorded by integration over the population over time. Since the populations are periodic we only need to integrate over one year.

There are two different ways to describe the way in which the temperature is recorded in the shells. On the one hand we can assume that the shell is built over the full life span of the creature. We can find then the recorded temperature by calculating the average living temperature:

$$(81) \quad T_{rec} = \langle T \rangle_R = \frac{\int_{1year} R(t)T(t)dt}{\int_{1year} R(t)dt}.$$

On the other hand we can assume that the shell is only produced during a short period after the birth of the animal. To calculate the recorded

Species $A$	$\bar{T}_A$ ( $^{\circ}C$ )	using (81)		using (82)	
		$T_{rec}$ ( $^{\circ}C$ )	$\bar{\delta}_R - \bar{\delta}_A$	$T_{rec}$ ( $^{\circ}C$ )	$\bar{\delta}_R - \bar{\delta}_A$
<i>G. ruber</i>	25	24.56	-	25.01	-
<i>G. bulloides</i>	12	22.35	-0.48	20.94	-0.89
<i>N. dutertrei</i>	20	22.24	-0.51	20.75	-0.94

TABLE 4. Temperatures recorded by the three species. The differences in  $\delta^{18}O$  are calculated using (68).

temperature we need to find the average reproduction temperature

$$(82) \quad T_{rec} = \langle T \rangle_R = \frac{\int_{1year} P_R(t) T(t) dt}{\int_{1year} P_R(t) dt},$$

where

$$P_R(t) = N\ell(R) \frac{1}{\sigma_R} e^{-\frac{(T-\bar{T}_R)^2}{2\sigma_R^2}}.$$

The result of the first evaluation is less sensitive to temperature effects, because the slow decay ( $e^{-\beta t}$ ) after a growth peak leads to an averaging out effect. In Table 4 we list the calculated temperatures for the simulation in Figure 9.

In Figure 10 we plot the recorded temperature as a function of the average sea water temperature  $T_0$ . The behaviour of the *G. ruber* population can be explained as follows. At low temperatures *G. ruber* will primarily grow during the NE monsoon when the temperatures are relatively high. Therefore at low temperatures *G. ruber* will record the maximum temperatures. At very high temperatures *G. ruber* will prefer the SW monsoon with its relatively low temperatures in combination with the large amount of nutrients present. In between these two regimes there is a transition around the optimal reproduction temperature of the species at 25 $^{\circ}C$ . The decrease in the recorded temperature in the transition region is explained by the availability of food. These effect are less pronounced in the left graph because of the averaging out effect.

**3.3. Reconstruction of historic temperatures.** To use this model for reconstruction of historic temperatures we perform a series of simulations on a grid of values for  $T_0$  and  $T_h$ . From each of the calculated populations we can then calculate the  $\delta^{18}O$  values recorded by these populations. These values are matched to the measured values. Note that since we know only two values from the measurements, we can only reconstruct two of the three variables we used to describe the temperature profile (80). Therefore we need to fix the value of  $\gamma$  and we cannot reconstruct the relative strength of the NE monsoon.

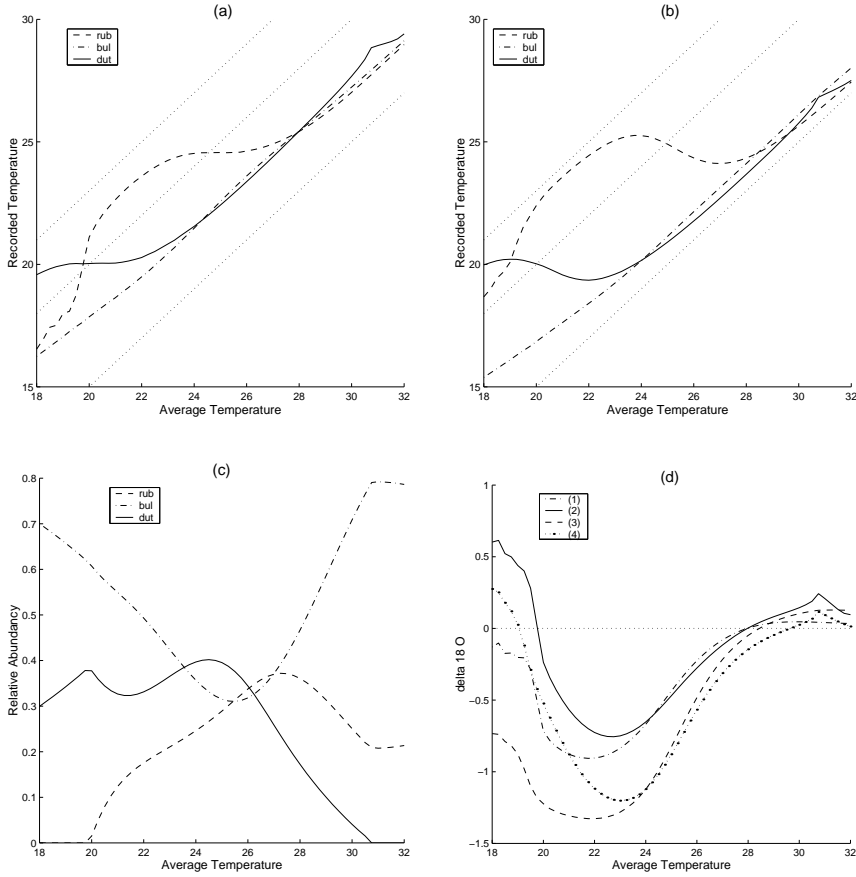


FIGURE 10. Response of the system to changes in the average temperature  $T_0$ . All other parameters are kept constant. (a) and (b) shows the average temperatures recorded by the three species, (a) is calculated using (81) and (b) is calculated using (82). The dotted lines in these figures show the average temperature and the minimum and maximum temperatures. (c) shows the relative abundance of the species and (d) shows the resulting differences in  $\delta^{18}\text{O}$ -values: (1)  $\delta^{18}\text{O}_R - \delta^{18}\text{O}_B$  using (81); (2)  $\delta^{18}\text{O}_R - \delta^{18}\text{O}_D$  using (81); (3)  $\delta^{18}\text{O}_R - \delta^{18}\text{O}_B$  using (82); (4)  $\delta^{18}\text{O}_R - \delta^{18}\text{O}_D$  using (82).

As a demonstration of this method we calculated the two  $\delta^{18}\text{O}$ -values on a uniform rectangular grid in  $(T_0, T_h)$  space. In Figure 11 we draw the contour graphs of the two resulting  $\delta^{18}\text{O}$  differences. So, if for example measurements give values of  $\delta^{18}\text{O}_R - \delta^{18}\text{O}_B = -0.75$  and  $\delta^{18}\text{O}_R - \delta^{18}\text{O}_D = -0.50$  we can reconstruct the historic temperature at the intersection of the corresponding contours in Figure 11. This

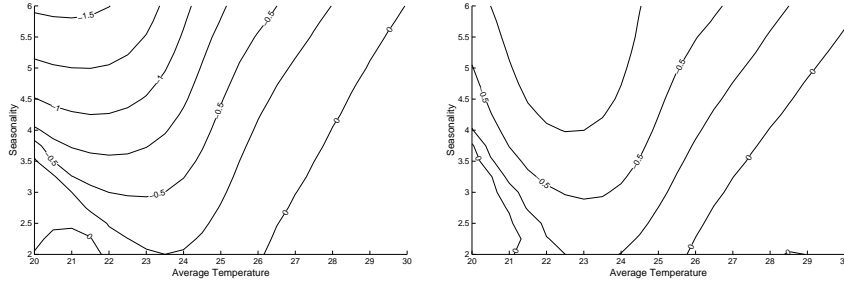


FIGURE 11. Contour graphs showing the effect of the average temperature and seasonality on the  $\delta^{18}\text{O}$  values. All other parameters are kept constant. The left graph shows  $\delta^{18}\text{O}_R - \delta^{18}\text{O}_B$ , the graph on the right shows  $\delta^{18}\text{O}_R - \delta^{18}\text{O}_D$ . Notice that these are related to the  $\delta^{18}\text{O}$ -differences in Figure 5(a) via a linear transformation.

approximately results in  $T_0 = 21^\circ\text{C}$  and  $T_h = 3.7^\circ\text{C}$ . Note that in this demonstration it is possible to estimate such intersection points only in a small part of the  $(T_0, T_h)$  domain. In most of the domain the contour lines are practically parallel, which makes it difficult to determine where they intersect, yielding inaccurate results.

It is possible to use the dynamic model to reconstruct the historic sea surface temperature analogous to the detailed results obtained for the basic model in section 2 (see Figures 6(a) and 6(b)), but we have not been able to pursue that here because of limited time resources.

#### 4. Discussion

Several detailed suggestions for further research are spread throughout the paper. Here we draw some more general conclusions.

- The interdisciplinary approach has been very beneficial in gathering new viewpoints. The use of even a fairly simple mathematical model can make a significant contribution in the determination of the sea surface temperature on the basis of the oxygen isotope composition of foraminifera.
- The model proposed in section 2, which incorporates seasonal effects, is a substantial improvement on models in which only the average temperature is considered.
- In order to obtain reliable quantitative information from the mathematical model(s) it is essential that the ecology of the foraminifera is understood in more detail.
- The incorporation in the model of effects related to nutrients and food availability does not lead to improvements; in fact the outcomes give unrealistic (negative) amounts of plankton. This may be due to

the way the food availability is incorporated in the model; further investigation is necessary.

- The process of secondary calcification (see section 1.5) can explain some of the present discrepancies between the experimental data and the outcomes of the model. However, quantitative information about this process is needed before a final conclusion can be drawn on this matter.
- Overall, the basic model of section 2 seems reasonable in its simplicity and the results agree (at least) qualitatively with what is known and expected. As a next step we suggest that an attempt is made to obtain more reliable values for the parameters in the model.
- The dynamic model, a system of coupled ordinary differential equations (see section 3), is a nice mathematical toy to investigate the influence of a variety of effects. The model is robust in the sense that the solution converges quickly to a yearly periodic cycle for a large range of parameter values. In principle it can be used to estimate the temperature and its variability from the experimental data. However, at present the level of sophistication of the ODE model is not in line with the relatively poorly constrained parameters derived from field observations and experimental data.
- From a scientific point of view it is essential that the sizes of the errors in both the experimental data and the values of the ecological parameters are determined. They should be taken into account when judging the reliability of the results of the analysis. This is also related to the amount of information that can be extracted reliably from the data.

### Acknowledgement

We would like to thank J. Hulshof and D. Nitzpon for their contributions to the discussions. We thank G.-J.A. Brummer for comments and helpful suggestions on a draft version of this manuscript.

### Bibliography

- [1] S.M.-H. Conan and G.-J.A. Brummer. *Fluxes of planktic foraminifera in response to monsoonal upwelling on the Somalia Basin margin*. Deep Sea Research, part II, 47: 2207–2227, 2000.
- [2] Ch. Hemleben, M. Spindler and O.R. Anderson. *Modern planktonic foraminifera*. Springer-Verlag, Berlin, 363 pp., 1989.
- [3] E.M. Ivanova. *Late Quaternary monsoon history and paleoproductivity of the western Arabian Sea*. Ph.D.-thesis, Vrije Universiteit, Amsterdam, The Netherlands, 172 pp., 1999.
- [4] S.-T. Kim and J.R. O'Neil. *Equilibrium and non-equilibrium oxygen isotope effects in synthetic carbonates*. Geochimica Cosmochimica Acta, 61, 3461–3475, 1997.

- [5] G.P. Lohmann. *A model for variation in the chemistry of planktonic foraminifera due to secondary calcification and selective dissolution*. *Paleoceanography*, 10(3): 445–457, 1995.
- [6] B.A. Malmgren, M. Kucera, J. Nyberg and C. Waelbroeck. *Comparison of statistical and artificial neural network techniques for estimating past sea surface temperatures from planktonic foraminifer census data*. *Paleoceanography*, 16, 1–11, 2001.
- [7] J.P. McCreary, K.E. Kohler, R.R. Hood and D.B. Olson. *A four-component ecosystem model of biological activity in the Arabian Sea*. *Progress in Oceanography*, 37: 193–240, 1996.
- [8] A. Mix. *The oxygen-isotope record of glaciation*. In: W.F. Ruddiman, H.E. Wright (Eds.), *North America and adjacent oceans during the last deglaciation (The Geology of North America, Vol. K-3)*. The Geological Society of America, 1987.
- [9] S. Mulitza, T. Wolff, J. Pätzold, H. Hale and G. Wefer. *Temperature sensitivity of planktic foraminifera and its influence on the oxygen isotope record*. *Marine Micropaleontology*, 33:223–240, 1998.
- [10] F.J.C. Peeters *The distribution and stable isotopic composition of living planktic foraminifera in relation to seasonal changes in the Arabian Sea*. Ph.D.-thesis, Vrije Universiteit, Amsterdam, The Netherlands. pp.184, 2000.
- [11] F.J.C. Peeters, G.-J.A. Brummer and G.M. Ganssen. *The effect of upwelling on the distribution and stable isotope composition of *Globerina bulloides* and *Globigerinoides ruber* (planktic foraminifera) in modern surface waters of the NW Arabian Sea*. *Global and Planetary Change*, in press.
- [12] E.R. Pianka. *Competition and niche theory*. In: R.M. May (Ed.), *Theoretical Ecology: Principles and Applications*. Oxford: Blackwells Scientific 1981, pp. 167–196.
- [13] G.A. Schmidt and S. Mulitza. *Global calibration of ecological models for planktic foraminifera from core-top carbonate oxygen-18*. *Marine Micropaleontology*, 44, 2002.
- [14] H.C. Urey *The thermodynamic properties of isotopic substances*. *Journal of the Chemical Society*, 562–581, 1947.